Corrosion-fatigue lifetime of Aluminium–Copper–Lithium alloy 2050 in chloride solution

M. Guérin [a,b], J. Alexis [b], E. Andrieu [a], C. Blanc [a], G. Odemer [a,*]

[a] Université de Toulouse, CIRIMAT, UPS/CNRS/INPT, 4 allée Emile Monso, BP 44362, 31030 Toulouse Cedex 4, France
[b] Université de Toulouse, INP/ENIT/LGP, 47 avenue d'Azereix, BP 1629, 65016 Tarbes, France

Keywords:
Aluminium–copper–lithium alloy
Fatigue endurance
Fatigue–corrosion
Corrosion morphology

A B S T R A C T

The fatigue behaviour of Aluminium–Copper–Lithium 2050 alloy under two metallurgical states (T34 and T84) was studied in air for healthy and pre-corroded samples in a 0.7 NaCl solution. The results were compared to those obtained during fatigue–corrosion tests performed in a similar chloride medium. Preliminary corrosion tests demonstrated that the T34 metallurgical state was susceptible to intergranular corrosion, while the T84 metallurgical state was susceptible to intragranular corrosion. Fatigue life tests in air on pre-corroded samples revealed a significant decrease in fatigue life related to the presence of corrosion defects before the cyclic solicitation. A strong effect of the first minutes of immersion in corrosive media was evidenced on fatigue life behaviour. The fatigue–corrosion tests revealed that the T34 metallurgical state was more affected by fatigue–corrosion in terms of fatigue life than the T84 metallurgical state. This observation can be explained by the increased propagation of intergranular corrosion enhanced by the cyclic solicitation.

1. Introduction

Due to their good mechanical properties and corrosion resistance, aluminium alloys are widely used in aeronautic applications. The strong increase in fuel price and environmental considerations caused the aluminium industry to develop a new generation of aluminium–copper–lithium alloys as an alternative solution. The addition of 1 wt.% lithium has been shown to induce a 3% decrease in the density and a 6% increase in the Young's modulus [1]. Among these alloys, the AA2050 alloy is a very promising material [2]; however, depending on its metallurgical state, localised corrosion features (pitting and intragranular or intergranular corrosion) can be observed due to its heterogeneous microstructure [3,4]. Indeed Al–Cu-Li alloys are precipitation-hardening alloys; the main strengthening phases can be T_1 (of nominal composition Al_2CuLi) and those of the θ′ sequence (with its metastable precursors) (Al_2Cu) [5]. Because intermetallic particles do not have the same electrochemical reactivity as the matrix, galvanic coupling can occur at the microstructural scale, leading to the localised corrosion morphology previously listed. Literature reported that T_1 precipitates are associated with corrosion phenomena in sodium chloride solutions [6–8]. Because they have a more negative corrosion potential than the matrix, they are associated with intergranular corrosion when they are present at grain boundaries, and with intragranular corrosion when they are present both at grain boundaries and in the grains [9]. Coarse intermetallic particles are mainly responsible for pitting [10,11].

Finally, aluminium alloys used in aircraft structures are susceptible to exposure to both corrosive environments and fatigue solicitations during their service life, thus inducing a decrease in their lifetime via corrosion–fatigue damage. Most studies have mainly focused on the fatigue–corrosion behaviour of the 2xxx (Al–Cu–Mg) aluminium alloys and less on the recent 2xxx (Al–Cu–Li) series. Richard et al. studied the role of microstructure and environment on the fatigue crack path of the AA2050-T851 alloy [12]. They found that the fatigue crack growth rate in ambient air was substantially accelerated in comparison with that in high vacuum. This result was explained by the role of water vapour and particularly by hydrogen-assisted crack propagation. The crack growth rate was correlated with fatigue crack morphology changes. Under vacuum conditions, the AA2050 alloy exhibited faceted and microscopically tortuous near-threshold fatigue crack paths. This deformation behaviour correlated well with the fatigue crack growth rate resistance resulting from the enhanced grain boundary barrier effect for slip bands and also crack branching and deviation.

Concerning the fatigue–corrosion damage and the impact on fatigue properties, most works focused on the 2xxx (Al–Cu–Mg) aluminium alloys and on the role of pre-corrosion damage on the residual fatigue life. Interactions between fatigue and corrosion are very rarely studied.

The reduction in the fatigue life after pre-corrosion tests is generally attributed to crack initiation from surface pits formed during a prior immersion in NaCl solution [13–18]. Dolley et al. demonstrated, for AA2024-T3, that the fatigue life was reduced by more than one order of magnitude after 384 h of pre-corrosion in a 0.5 M NaCl solution compared to that of uncorroded specimens. The reduction of fatigue life was related to the time of exposure to the corrosive environment

* Corresponding author.
E-mail address: gregory.odemer@ensiacet.fr (G. Odemer).

and the pit size [18]. Indeed, corrosion pits provide potential stress concentrator sites at which fatigue cracks can initiate. The pit size (average depth and width) seems to be an essential parameter; the fatigue life was successfully predicted by 2D AFGROW (Fracture Mechanics and Fatigue Crack Growth Analysis software tool) calculations based on initial crack sizes similar to those of pits [19].

All of these studies have considered premature fatigue crack initiation induced by pitting corrosion, which is one of many possible localised corrosion morphologies. Pauze studied fatigue crack initiation on another type of localised corrosion defect, i.e., intergranular corrosion defects for an AA2024-T351 aluminium alloy [20]. She observed that intergranular corrosion defects, as well as pits, acted as preferential initiation sites for transgranular fatigue cracks. She concluded that at the surface of the material, application of a cyclic stress induced the coalescence of either semi-elliptical intergranular corrosion defects or semi-elliptical fatigue cracks initiated on intergranular corrosion defects. Thus, the fatigue–corrosion studies in the literature have highlighted the major role of localised corrosion defects on premature fatigue crack initiation. The morphology of these localised corrosion defects is essential in determining the time to crack initiation; this result implies that precisely characterising a material's corrosion defect morphology, related to its metallurgical state resulting from the shaping process, will provide insight into crack initiation. In this way, Turnbull has characterised the pit-to-crack transition by means of X-ray computed tomography (XCT) and focused ion beam machining with scanning electron microscopy (FIB–SEM) combined with Finite Element analysis [21]. He has shown an acceleration of growth rates for short cracks under fatigue loading that can be attributed to an electrochemical crack size effect. The location of crack initiation probably depended on the near-surface microstructure, hardness and residual stress. Burns et al. have studied the fatigue crack formation from a corroded AA7075-T651 which involves a complex interaction of elastic stress concentration due to three-dimensional pit macro-topography coupled with local micro-topographic plastic strain concentration, further enhanced by microstructure [22,23].

In this paper, the effect of pre-corrosion damage and the synergistic impact of fatigue–corrosion on fatigue life was studied for a AA2050 alloy in two different metallurgical states, i.e., naturally aged (T34) and artificially aged (T84) because, depending on the metallurgical states, different corrosion morphologies, namely intergranular and intragranular corrosion, were observed for T34 and T84, respectively. The comparison of the fatigue behaviour for the two metallurgical states allowed for identification of the critical microstructural parameters responsible for the strong decrease in fatigue lifetime. The fracture surfaces observed from the different tests for each microstructure were explained based on the microstructure and corrosion susceptibility of the different metallurgical states.

2. Materials and methods

2.1. Material

The material was an aluminium–copper–lithium 2050 alloy (Al base, 3.86% Cu, 0.86% Li, wt %) provided by Constellium (France). It was received as a 50-mm-thick plate obtained by hot rolling, followed by solutioning, water quenching, stretching and natural ageing at room temperature, leading to the T34 metallurgical state. In this metallurgical state, according to the literature, hardening T_1 precipitates were not present in the grains [24]. To study the influence of an ageing treatment on the corrosion and fatigue–corrosion behaviour of the AA2050 alloy, and particularly the role of hardening T_1 precipitates, T34 samples were aged at 155 °C for 30 h, leading to a T84 metallurgical state [25].

Due to the rolling process, the microstructure of both T34 and T84 sheets presented high anisotropy. Observations by optical microscopy (OM) of the thick plate revealed grains strongly elongated in the rolling direction. Their average sizes in the long transverse (LT) and short transverse (ST) directions were 350 μm and 60 μm, respectively, with a large discrepancy in size from one grain to another. In the longitudinal (L) direction, the discrepancy is such that the calculation of a mean value is not significant. A thinner analysis by electron back scattering diffraction (EBSD) revealed two populations of grains, i.e., a population of large polygonised grains (size varying from 350 μm to 5 mm in the L direction) and another one of recrystallised grains of smaller dimensions (between 5 μm and 20 μm in the L direction) [26]. In this study on fatigue–corrosion, the (L-LT) plane was selected by industrial partner. So results presented in this paper are available for this plane given that corrosion morphology and corrosion propagation can be modified according to the exposed plane.

Scanning electron microscopy revealed the presence of coarse Al–Cu–Mn–Fe particles for T34 and T84 samples. Their density and distribution (both in the grains and at the grain boundaries) were similar for the two metallurgical states. These particles mainly influence the susceptibility to pitting corrosion of the alloy. The finer precipitation, responsible for intergranular and intragranular corrosion, was described precisely in previous works [25,26]. In summary, for the T34 metallurgical state, T_1 precipitates were neither observed in the grains nor at the grain boundaries, despite its susceptibility to intergranular corrosion; for T84 metallurgical states, T_1 precipitates were observed both in the grains and at the grain boundaries [26].

2.2. Tensile tests

Tensile tests were performed on tensile specimens using an MTS testing machine equipped with a 5 kN load cell at a constant strain rate of 10^{-3} s^{-1} to determine the yield strength (YS) and thus fix the choice of the different stress levels applied for fatigue tests.

2.3. Corrosion tests

Corrosion tests were performed on a cubic sample (1 cm edge) in a 0.7 M NaCl solution at room temperature (25 °C) during continuous immersion (CI) times of 24 h, 72 h and 168 h. The (L–LT) plane was exposed to the electrolyte according to the exposition plane of fatigue samples (see below). Taking into account the grain morphology, the corrosion defects preferentially propagated in the L and LT directions. After performing the corrosion tests and the optical microscope observations of the exposed (L–LT) plane, each cubic sample was cut along the (LT–ST) plane and then observed. To describe the corrosion morphology, more than 7 cm of sample were analysed in the LT direction. Three parameters were statistically determined: the average propagation of corrosion defects in the ST direction (defect depth), the average propagation of corrosion defects in the LT direction (defect width) and finally the linear density of corrosion defects in the LT direction (number of corrosion defects per mm).

2.4. Fatigue and fatigue–corrosion tests

Stress-controlled uniaxial fatigue tests were conducted at 25 °C, in ambient air or in a 0.7 M NaCl aerated solution, on a precision-aligned fatigue machine (BOSE ElectroForce 3330®). The fatigue sample shape is shown in Fig. 1. The sample surface and edges were mechanically abraded up to 4000 grade, polished with 3-μm and 1-μm diamond pastes, and then rinsed in distilled water and air-dried. Before performing the fatigue tests in air, some samples were pre-corroded, which, as in the corrosion tests previously described, consisted of 48 h or 72 h of continuous immersion in a 0.7 M NaCl aerated solution at room temperature (25 °C). Only 1 cm in the middle of the samples on both faces (L–LT plane) was exposed to the corrosive media to localise the rupture in the centre of the sample. Concerning fatigue–corrosion tests, a specific test bench was designed. This bench was composed of a leak-tight corrosion cell adapted to the fatigue machine in which the corrosive solution was continuously circulated by a peristaltic pump. A

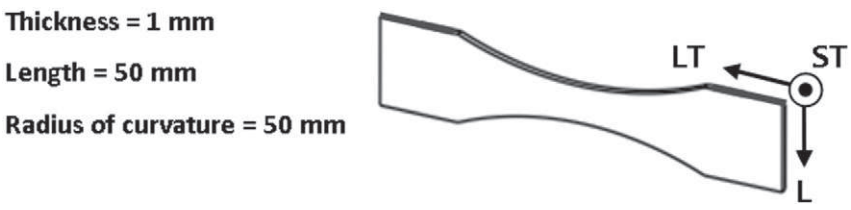

Fig. 1. Fatigue sample geometry.

Julabo® refrigerated/heating circulator was used to control the temperature (25 °C) of the electrolyte in the corrosion cell via an external Pyrex® thermal exchanger.

Fatigue life and fatigue–corrosion life tests were performed using a 20 Hz sine wave with a stress ratio of R = 0.1 (with R = σmin/σmax). The results of these tests are presented as a plot of stress level (σ) as a function of the number of cycles to failure (N) (S–N curves). Several stress levels (from 40 to 90% of YS) were considered, according to the YS preliminarily determined for each metallurgical state.

2.5. Scanning electron microscope (SEM) observations

Scanning electron microscopy (LEO-435-VP) was performed with an incident electron beam between 10 kV and 15 kV to carefully examine the corrosion defects and the fracture surfaces obtained after tensile and fatigue and/or fatigue–corrosion tests.

3. Results and discussion

3.1. Preliminary characterisation

3.1.1. Corrosion behaviour of AA2050 during continuous immersion tests

The corrosion behaviour of AA2050 was studied in previous works for the T34 and T84 metallurgical states [25,26]. After the CI tests, observations of the (L–LT) plane revealed the presence of pitting corrosion at the surface of T34 and T84 samples for all immersion times. An example is given in Fig. 2 for the T34 metallurgical state and for an immersion time of 72 h. This type of corrosion is due to galvanic coupling between second phase particles, usually rich in copper, such as Al–Cu–Fe–Mn intermetallic particles, and the matrix. These particles cause the dissolution of the surrounding matrix because of their nobler electrochemical potential [10,11]. As this type of corrosion was not studied in detail in previous works, it is important to notice some important remarks:

- at the corrosion potential, the corrosion kinetics is limited by the oxygen reduction kinetics. Thus, the development of pits can limit the propagation of intra/intergranular corrosion;
- the distribution of coarse intermetallic particles can be different from one sample to another. Thus, the pit density can vary from one sample to another, which can modify the intra- or intergranular defect density;
- as stated in the previous part, pits are preferential sites of fatigue crack initiation.

Furthermore, after the CI tests, T34 samples were found to be susceptible to intergranular corrosion (Fig. 3). In contrast with the literature, for the material studied in the T34 metallurgical state, no T_1 precipitates were observed at grain boundaries. Intergranular susceptibility was reported to be caused by a preferential segregation of alloying elements, i.e., most likely Cu and/or Li, at grain boundaries as well as heterogeneities at the polycrystal scale [27]. For T84 samples, corrosion was mainly intragranular (Fig. 3) [25,26]. It was shown that T_1 precipitation was abundant as well in grains as at grain boundaries. At grain boundaries, T_1 precipitation was continue and did not lead to the formation of a precipitate free zone.

Proton et al. have studied the influence of an ageing treatment on the corrosion susceptibility of AA2050 alloy [9]. The corrosion potential of T84 metallurgical state was strongly lower than that of T34 according to results of literature [19]. This decrease was related to the precipitation of T_1 phase in the grains which therefore had a more negative corrosion potential than the grains of T34 metallurgical state. Moreover, the copper content of the solid solution of the heat-treated state decreased due to the precipitation of T_1 phase which contributed to explain the decrease of the corrosion potential of the grains for the T84 metallurgical state. A galvanic micro-coupling occurred between the matrix and T_1 phase present in the grains leading to a homogenous dissolution of the grains (intragranular corrosion). On the contrary, due to the presence of numerous T_1 precipitates in the grains, the galvanic coupling between grains and grain boundaries was less severe for T84 than for T34 samples leading to the desensitization of T84 state to intergranular corrosion [28,29].

The statistical analysis of the corrosion morphology was conducted in the (LT–ST) plane to quantify the defect depth (ST direction) and

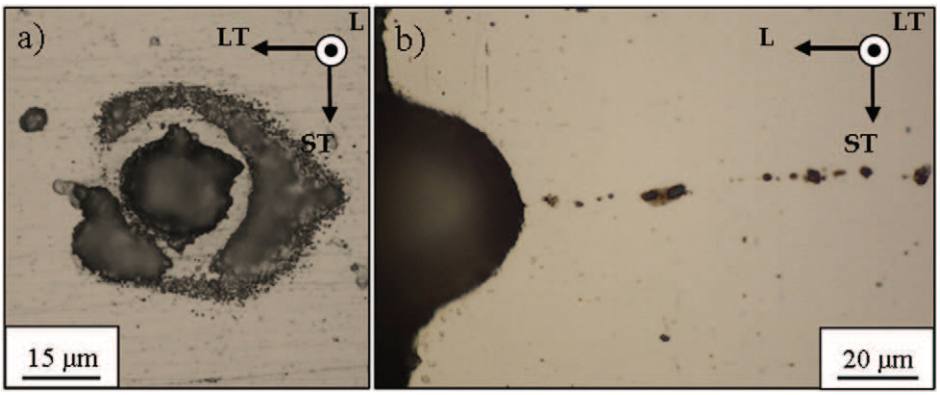

Fig. 2. Optical micrographs of pits for the T34 AA2050 sample after CI for 72 h: a) at the surface; b) cross-section. ((LT–ST) plane exposed to the electrolyte for this experiment).

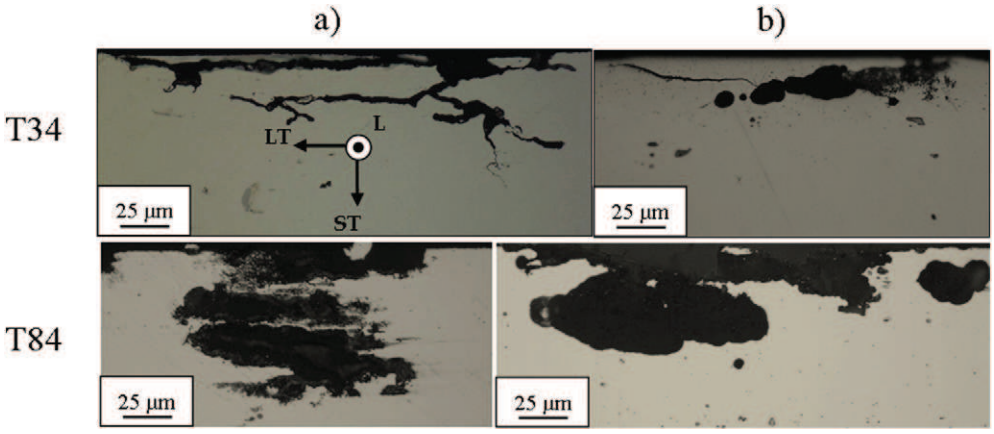

Fig. 3. Optical micrographs of the corrosion defects for T34 and T84 samples: a) after CI for 24 h and b) after CI for 72 h.

their width (LT direction) for both T34 and T84 samples (Fig. 4). For the T34 metallurgical state, the results indicated that intergranular corrosion propagation in the LT direction was strongly slowed after 24 h of immersion time. This decrease of the propagation of the intergranular corrosion defects with the immersion time is generally related, on the one hand, to the oxygen depletion of the corrosive medium particularly consumed by initiation and propagation of defects (intragranular or intergranular and pits) and, on the other hand, to the accumulation of the corrosion products during the test [30,31]. In this way, a competition between initiation and propagation of corrosion defects should explain the slowdown of propagation. Indeed, the statistical analysis revealed that the defect density increased until 48 h of immersion time (Fig. 4). Moreover, it is important to remember that the strong variation of grain size in the LT direction could have an effect on the corrosion defect propagation related to the presence of small grains and to the difference of crystallographic parameters of grain boundaries as shown in a previous work [26].

For the T84 metallurgical state, the evolution of intragranular corrosion damage is relatively similar to the evolution of intergranular damage for the T34 metallurgical state. A rapid propagation of corrosion defects in the LT and ST directions is observed for the first 24 h, followed by a slower velocity (Fig. 4a). The maximal density of corrosion defects is reached very quickly (Fig. 4b).

For both metallurgical states, in addition to the oxygen depletion and the accumulation of corrosion products, the slowdown of the defect propagation was strongly related to the anisotropic grain morphology. For intragranular corrosion, i.e., the T84 metallurgical state, grain boundaries acted as a barrier to propagation. For intergranular corrosion, i.e., the T34 metallurgical state, propagation was favoured in the L direction. Obviously, these differences between the morphology of corrosion of the T34 and T84 metallurgical states are an important factor from a fatigue and fatigue–corrosion crack initiation point of view.

3.1.2. Tensile behaviour of AA2050

To choose the relevant stress levels to apply for fatigue and fatigue–corrosion tests, preliminary tensile tests were conducted at 25 °C on healthy samples for the T34 and T84 metallurgical states (ISO 6892–1 International Standard). The tensile mechanical characteristics are summarised in Table 1. Ageing treatment caused the formation of hardening T_1 precipitates, thereby inducing an increase in the yield strength and the ultimate tensile strength at the expense of the ductility, i.e., the elongation to failure for the T84 samples compared to the T34 samples. These observations are consistent with other works on AA2050 [30–32].

The corresponding fracture surfaces were observed by SEM and are presented in Fig. 5 only for the T84 metallurgical state for clarity, given that the rupture surfaces of the T34 metallurgical state are similar. These observations revealed a main ductile rupture characterised by dimples but with a strong effect of the microstructure on fracture surfaces with the presence of intergranular decohesion phenomena due to the crystallographic and/or morphologic anisotropy of the sheet issued from the rolling step (Fig. 5a). The effect of grain misorientation on the dimple orientation was clearly observed in Fig. 5b.

3.1.3. Fatigue endurance behaviour of AA2050

Fatigue life curves of healthy samples are presented in Fig. 6 for each metallurgical state. To compare the two metallurgical states, Fig. 6a shows the evolution of the maximum stress level (calculated by comparison with the YS of the tensile sample to take into account the evolution of the mechanical properties related to the ageing treatment) vs. cycles to failure. Fig. 6b shows the maximum stress level in MPa vs. cycles to failure.

For a given stress level, and taking into account the effect of heat treatment on tensile mechanical properties, these curves showed that heat treatment led to a strong decrease in fatigue life (approximately one order of magnitude). The endurance limit decreased by 25% with the ageing treatment. However, if the stress level is considered in terms of the effective stress in MPa, then the fatigue endurance results of the T34 and T84 metallurgical states were very similar for low stress levels. Nevertheless, the T84 metallurgical state was able to support stress levels higher than the T34 metallurgical state, according to tensile results in relation with the microstructural changes (formation of hardening T_1 precipitates).

Fig. 7a shows the fracture surface observed using SEM for a T84 metallurgical state which is roughly similar to the fracture surfaces obtained for T34 metallurgical state. Independent of the stress levels, the fracture surfaces presented three distinct zones characterised by different rupture modes: the zone of crack initiation (less than 1% of the area of the rupture surface, for an average size of corrosion defect of 20 µm), the zone of crack propagation (around 65% of the area of the rupture surface) and the zone corresponding to the final rupture (around 35% of the area of the rupture surface). Crack initiation was always localised on coarse intermetallic particles for both metallurgical states (Fig. 7b). Indeed, crack initiation was due to the localisation of plasticity on coarse particles, leading to their shearing. The final rupture zone was characterised by dimples and by the presence of microcracks along grain boundaries elongated in the L direction (Fig. 7c and d).

A transgranular propagation mode was observed for both metallurgical states, characterised by flat-facets and step-like patterns. (Fig. 7a, c and e). These rupture modes were consistent with the works of Richard et al. [12], Ro et al. [33,34] and Slavik et al. [35] on the effects of environment, microstructure and texture on fatigue crack facet orientation and fatigue crack growth for, respectively, a 2050-T851 aluminium alloy and 2090 Al–Cu–Li–Zr and C47A-T86

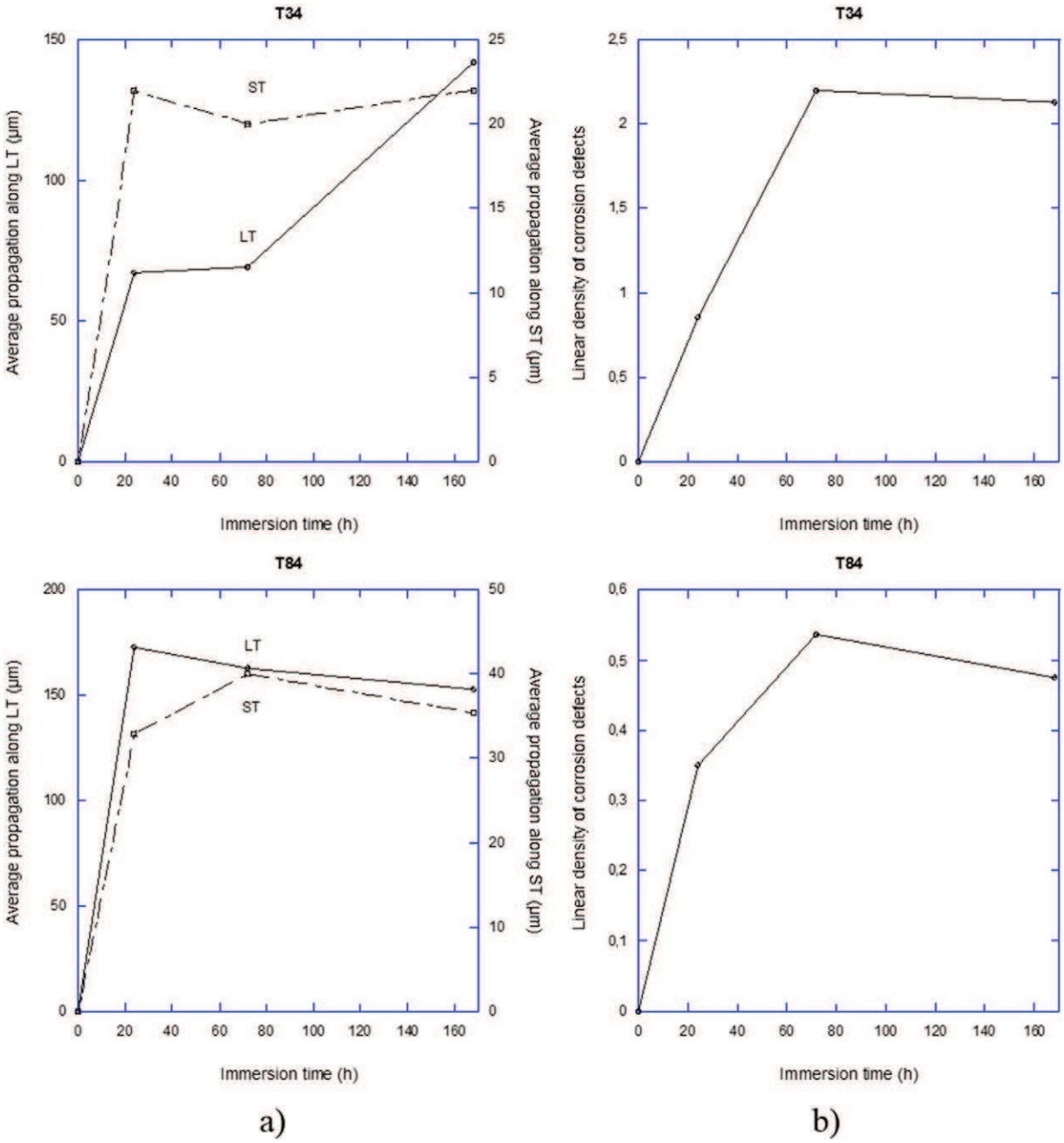

Fig. 4. Evolution of corrosion morphology with immersion time for T34 and T84 metallurgical states: a) average propagation of corrosion defects along the ST and LT directions; b) linear density of corrosion defects (number of defects/mm).

Al–Cu–Li alloys. So Ro et al. have observed, in ultra-high vacuum, faceted and tortuous fracture crack paths, identified as near-{111} surface facets associated with slip-band cracking. This may be understood mechanistically in terms of slip localization induced by T_1 shearable precipitates in the Al–Cu–Li aluminium alloys [12,33,34,36,37]. This deformation behaviour correlated with good fatigue crack growth resistance resulting from enhanced grain boundary barrier effect for slip bands and also crack branching and deviation.

In humid environment, a crack path transition was observed, characterised by areas of flat-facet and step-like features. Detailed analysis of such features in C47A-T86 established that there was a complex array of surface orientations that span from {100} to {110} [12,33,34]. It was suggested that hydrogen enhanced lattice decohesion across both low and high index planes, as well as dislocation cell structure embrittlement, each controlled by local normal stress that depends on grain orientation.

Table 1
Tensile mechanical properties of the AA2050-T34 and -T84 alloy at 25 °C.

	Yield strength (MPa)	Ultimate tensile strength (MPa)	Elongation to failure (%)
T34 metallurgical state	280	470	20
T84 metallurgical state	520	590	10.5

3.2. Effect of corrosion on the fatigue life properties in air

To better understand fatigue–corrosion interactions, first, the effect of pre-corrosion damage on fatigue life and fracture modes must be

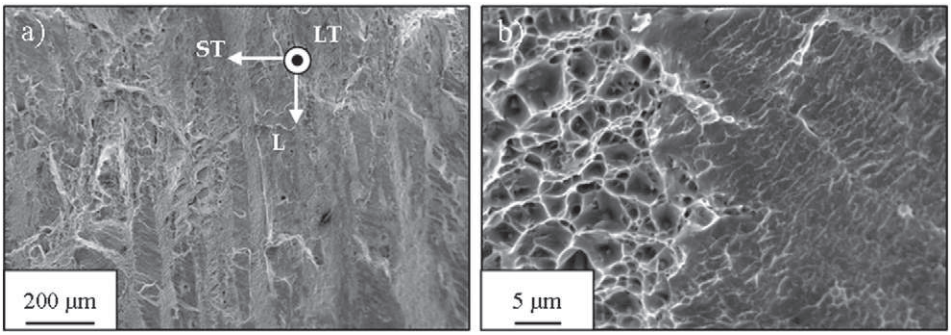

Fig. 5. Rupture surfaces observed using SEM of the T84 metallurgical state: a) delamination phenomenon; b) interface between two misoriented grains covered by dimples.

characterised. The fatigue life curves plotted after a 72 h pre-corrosion immersion are presented in Fig. 8a and b for the T34 and T84 metallurgical states, respectively.

Fatigue life of 72 h pre-corroded samples was reduced by approximately 80% compared to the uncorroded samples for each metallurgical state. The representation of the maximal stress level vs. the number of cycles to failure revealed that the two metallurgical states exhibited similar fatigue life behaviour after pre-corrosion treatment (Fig. 8c) suggesting that the corrosion morphology, i.e. intergranular and intragranular for T34 and T84 respectively, should not affect the fatigue life behaviour.

The corresponding fracture surfaces observed using SEM are presented in Fig. 9. The fracture surfaces are very similar for both the T34 and T84 metallurgical states. A multi-crack initiation is observed from corrosion defects appearing during pre-immersion. According to the study of corrosion behaviour presented in the preliminary characterisation part, SEM observations of fracture surfaces showed the corrosion defects initiating the fatigue cracks were intergranular for the T34 metallurgical state and intragranular for the T84 metallurgical state (Fig. 9). Except for the nature of the initiation sites, the fracture surfaces were similar for both pre-corroded and healthy samples; therefore, the fracture surfaces were similar for the two metallurgical states and were the same as for the fatigue tests on healthy samples, suggesting that the fracture modes were not affected significantly by the corrosion morphology or by the hydrogen produced during corrosion processes.

Most of the previous studies focused on the fatigue crack initiation from only one localised corrosion morphology, i.e., pitting corrosion. These studies indicated that the pit size, i.e., width and length, was a critical parameter; in addition, the repartition and inter-spacing of pits on the sample surface, which could induce multiple crack initiation and finally result in their coalescence, are other critical parameters [23,38–41]. In a recent work, corrosion-to-fatigue crack transition was analysed in detail by Burns et al. for AA7075-T651 [22]. So, it was shown that pit macro-topography produced significant elastic stress concentration that degraded fatigue crack formation and early growth resistance at a length scale (≈250 µm) intermediate between surface constituent particle nucleated fatigue (≈10 to 50 µm) and damage tolerant flaw size (1300 µm). Crack formation was further promoted, and dominated, due to interaction of driving forces local to the perimeter of the pit, including micro-topographic plastic strain concentration augmented by constituent particles below the pit surface.

If it is possible to compare pits to intragranular corrosion defects, it is more difficult to arrive at a conclusion about the effect of intergranular corrosion defects on fatigue crack initiation. Generally, intergranular corrosion defects are thinner and longer than intragranular defects, and a new parameter, such as the crack-tip-acuity effect on crack initiation, should be taken into account. However, in the present work, the results of fatigue life tests on pre-corroded samples have shown that the T34 and T84 metallurgical states have a similar behaviour. Corrosion tests (Fig. 4) revealed that the evolution of the average propagation in the ST direction was relatively similar for the T34 and T84 metallurgical

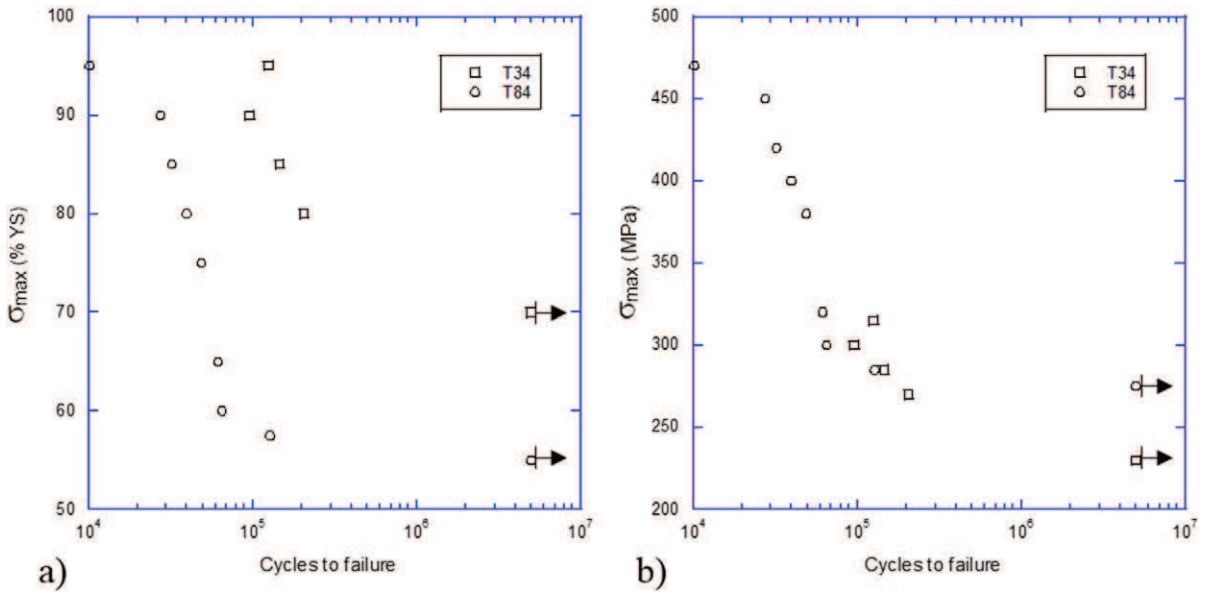

Fig. 6. Fatigue life curves of AA2050-T34 and -T84 in air at 20 Hz R = 0.1: a) σmax (% YS) vs. number of cycles to failure; b) σmax (MPa) vs. number of cycles to failure.

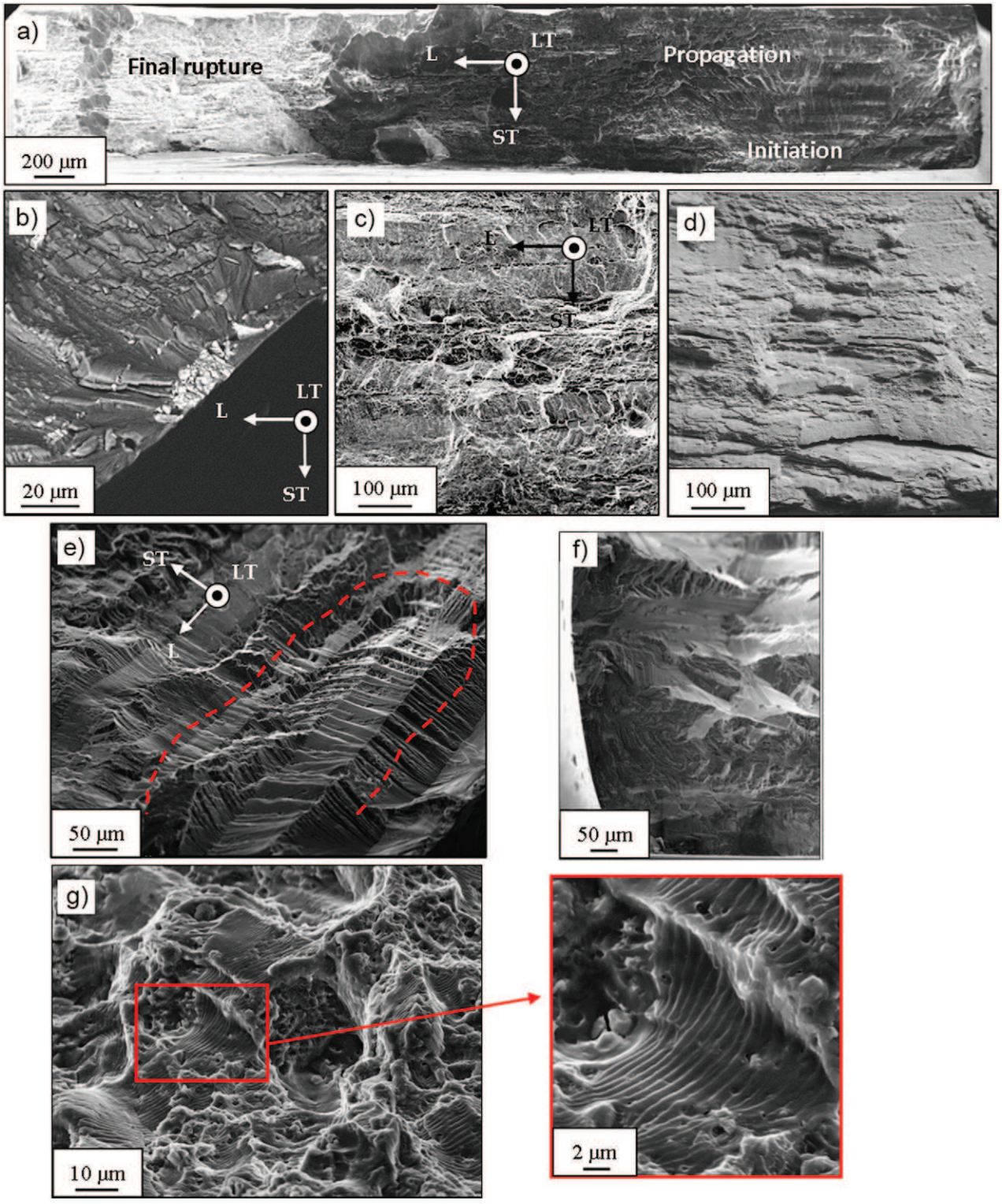

Fig. 7. SEM micrographs of the fatigue fracture surfaces of AA2050 tested in air at 20 Hz R = 0.1 for a stress level of 80% YS: a) global view (T84); b) initiation zone (T84); c) delamination propagation zone (T84); d) delamination at a small scale (T84); e) transgranular propagation zone (T84); f) transgranular propagation zone (T34); g) striation (T34).

states given that the statistical analysis should be slightly imprecise due to the observation plane chosen and the types of morphologies seen, but the values were slightly higher for T84 compared to T34. Moreover, corrosion defect density was more important for the T34 material. Whatever the metallurgical state, similar fatigue life results were obtained for a 24 h pre-corrosion treatment compared to a 72 h pre-corroded sample. This should be related to the constant average propagation in the ST direction between the cases of pre-immersion of 24 h and 72 h. The results suggest that the corrosion defect density and morphology, i.e., intra- or intergranular, were not predominant parameters for these long pre-immersion times. Only the length of corrosion defects in the ST direction should control the crack initiation but a critical length of corrosion defects could be defined; according to statistical analysis, this critical length is less than 20 µm for both metallurgical states. To

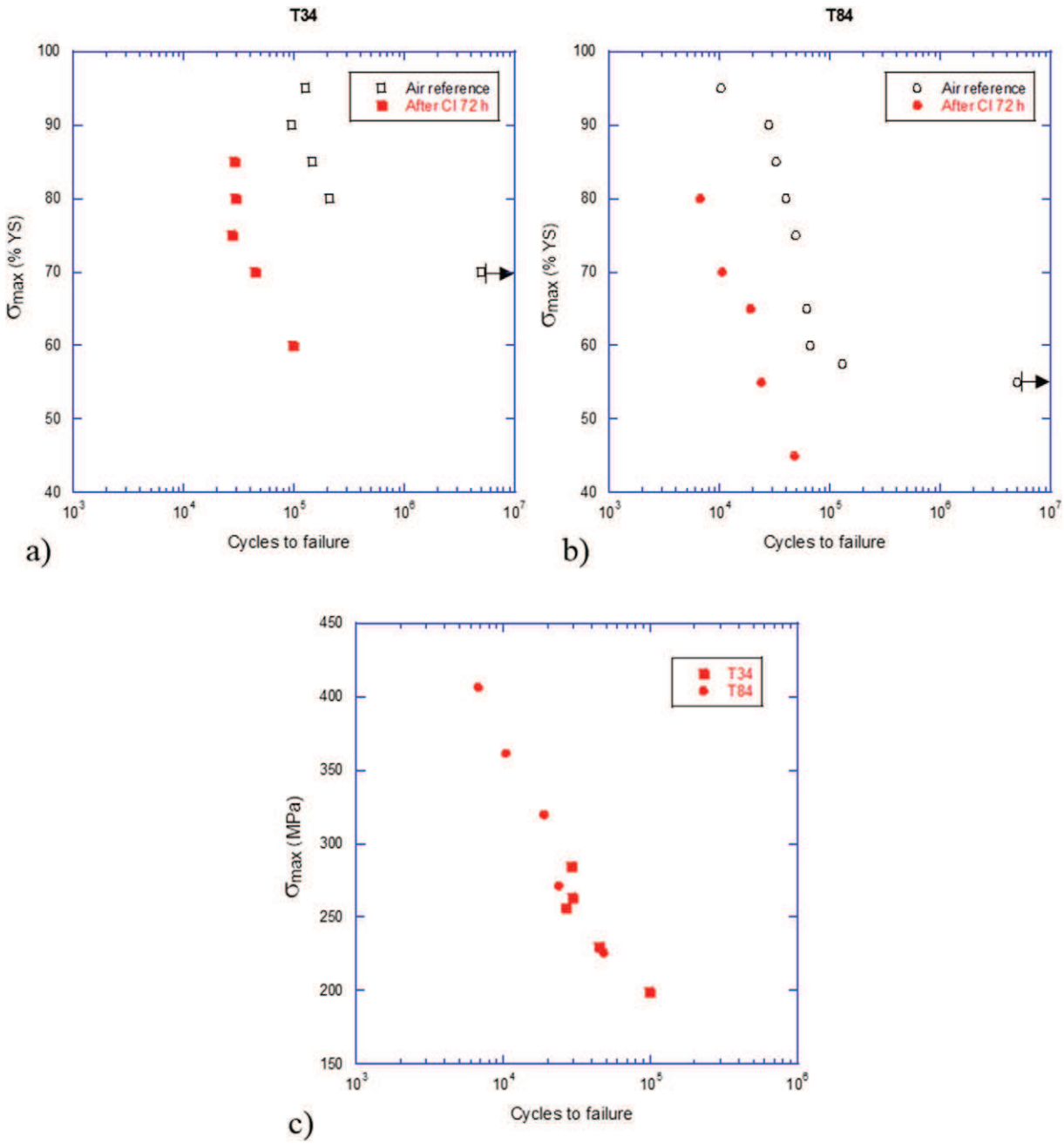

Fig. 8. Fatigue life curves (σmax (% YS) vs. number of cycles to failure) in air at 20 Hz R = 0.1 for 72 h pre-corroded samples: a) T34 metallurgical state; b) T84 metallurgical states; and c) fatigue life curves (σmax (MPa) vs. number of cycles to failure) in air at 20 Hz R = 0.1 for 72 h pre-corroded samples of the T34 and T84 metallurgical states.

statute on this point, it would be necessary to analyse precisely the initiating feature and study some relevant parameters such as 3D-morphology of corrosion defects and local micro-topographic plastic strain concentration, further enhanced by microstructure.

However, for shorter times of pre-corrosion, the fatigue results could be different. Indeed, the statistical analysis indicated that the average propagation evolved rapidly for short times of less than 24 h. In this case, the corrosion morphology could play a role on crack initiation if the corrosion defect critical length was not reached during pre-immersion treatment, particularly if a fatigue solicitation occurred at the same time. The effect of short pre-corrosion times on corrosion damage assisted or not by fatigue solicitation will be discussed later in this paper and compared to other works on this issue [23,42,43].

3.3. Corrosion–fatigue life behaviour

The results of fatigue life tests performed in corrosive media, i.e., 0.7 M NaCl solution, at 25 °C are presented in Fig. 10 for the T34 and T84 metallurgical states. For each fatigue test, the corresponding time spent in the media until rupture is indicated on the figure in minutes. The results of fatigue on samples pre-corroded for 72 h are also shown for comparison.

The results indicated that fatigue–corrosion induced a decrease in fatigue life for both the T34 and T84 metallurgical states. For the T34 metallurgical state, the decrease was similar to the decrease observed for fatigue tests on samples pre-corroded for 72 h. However, the immersion times spent in the media were much shorter, i.e., from 20 min to 75 min for a maximal stress level (in % of YS) varying from 50% to 90%. For the

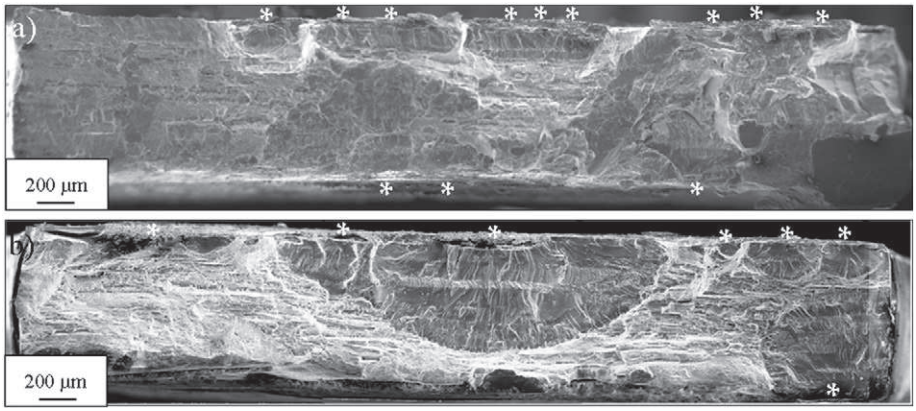

Fig. 9. SEM micrographs of fatigue fracture surfaces of AA2050 tested in air at 20 Hz R = 0.1 for a stress level of 80% YS after a 72 h pre-corrosion treatment: a) T34 state; b) T84 state. White stars indicate the initiation zones.

T84 metallurgical state, the tendency was the same, except that the fatigue–corrosion life is slightly better than the fatigue life of the samples pre-corroded for 72 h.

Two assumptions are used to explain these first results:

- a synergistic effect between fatigue and corrosion occurred for the two metallurgical states. The fatigue contribution during fatigue–corrosion tests should help the localised corrosion, i.e., intra- or intergranular corrosion according to the metallurgical state considered, to prematurely appear by embrittlement of the oxide passive layer. Note that fatigue enhanced the corrosion defect propagation until a sufficient critical length was achieved, thus inducing fatigue crack initiation. Concerning this point, a mechanism proposed by Delafosse et al. [44] was based on hydrogen/dislocation interactions that emphasised the cooperative effects of corrosion and plasticity. However, in this study, this type of mechanism was very unlikely due to the short time spent in the corrosive media and the likely small cathodic hydrogen amount produced;
- the second assumption is that the first moment spent in the corrosive media was sufficient to lead to the formation of corrosion defects important enough to induce fatigue crack initiation (pits or inter- or intragranular defects). The critical immersion time susceptible to induce these defects appeared to be approximately 15–20 min. To validate this point, some additional fatigue tests were conducted on pre-corroded samples for short immersion times corresponding to the fatigue–corrosion test times. These test results will be presented later in this paragraph.

Fig. 11 presents the SEM micrographs of the fracture surfaces obtained after fatigue–corrosion endurance tests for the T34 and T84 metallurgical states. Analogous to the fatigue tests performed on pre-corroded samples, crack initiation was localised on corrosion defects whose sizes were smaller than corrosion defect sizes observed on pre-corroded samples, according to the time spent in the corrosive media (10 µm for the length and 450 µm for the width for the T34 metallurgical state and 15 µm for the length and 180 µm for the width for the T84 metallurgical state for a maximal stress level of 50% of YS). The intragranular corrosion defects of the T84 metallurgical state are not as wide as the intergranular corrosion defects of the T34 metallurgical state, which should explain the difference in fatigue life. Concerning the rupture mode, the same mechanisms were observed in the initiation and propagation zones.

3.4. Interaction between corrosion and fatigue damage

To determinate if, effectively, fatigue–corrosion interactions occurred during cyclic mechanical tests, some additional fatigue tests were conducted on pre-corroded samples for short immersion times corresponding to the fatigue–corrosion test times. These tests are presented in Fig. 12. For the T34 metallurgical state, the results indicated that for an equivalent time spent in corrosive electrolyte, the fatigue life decreased under fatigue–corrosion coupling compared to the fatigue tests on pre-corroded samples. This result suggested that a fatigue–corrosion synergy occurred for the T34 metallurgical state, contrary to the T84 metallurgical state that presented the same decrease in fatigue life on pre-corroded samples as under fatigue–corrosion conditions.

SEM observations of the fracture surfaces of the T84 metallurgical state have shown no difference between the fatigue–corrosion and the fatigue tests on the pre-corroded samples. However, the SEM images of the fracture surfaces of the T34 metallurgical state obtained after fatigue tests for a 75′ pre-corrosion treatment revealed a significant change in the size of intergranular corrosion defects where the fatigue crack initiated. In the fatigue–corrosion decoupling situation, i.e. fatigue tests on pre-corroded samples, corrosion defects were always smaller than under fatigue–corrosion conditions, which suggested that fatigue solicitation contributed to the propagation of intergranular corrosion defects maybe by an embrittlement of the passive oxide layer at the tip of corrosion defects due to local plastic mechanisms. This assumption was not true for the T84 metallurgical state, which presented another type of corrosion defect, i.e. intragranular corrosion, which demonstrated the primordial role of corrosion morphology on the existence or non-existence of the fatigue–corrosion interaction. This finding has already been observed under stress corrosion cracking for a monotone stress in a previous work [26] and by Pauze et al. for cyclic solicitation [20].

Beyond this fatigue–corrosion issue, note the strong effect of the first minutes of immersion in corrosive media on fatigue life behaviour. For example, a pre-corrosion treatment of 15 min induced the same decrease in fatigue life as a pre-corrosion treatment of 72 h for the T84 metallurgical state for a stress level of 80% of YS. This observation was in good agreement with previous work regarding corrosion initiation during the first moments of immersion [26]. Indeed, open circuit potential (OCP) measurements have shown a fast and strong reactivity of the alloy during the first moments of immersion in 0.7 M NaCl solution. The stabilization was related to the accumulation of corrosion products on the surface. These results were corroborated by electrochemical impedance spectroscopy (EIS) measurements.

Finally, for fatigue tests performed on pre-corroded samples, fatigue crack initiation was directly related to a critical length of corrosion defect (reached on the basis of this work after only 15–20 min), whatever the corrosion morphology, i.e. intergranular for the T34 metallurgical state and intragranular for the T84 metallurgical state. Under fatigue–corrosion conditions, the corrosion morphology played an important role in crack initiation, given that fatigue enhanced the propagation of

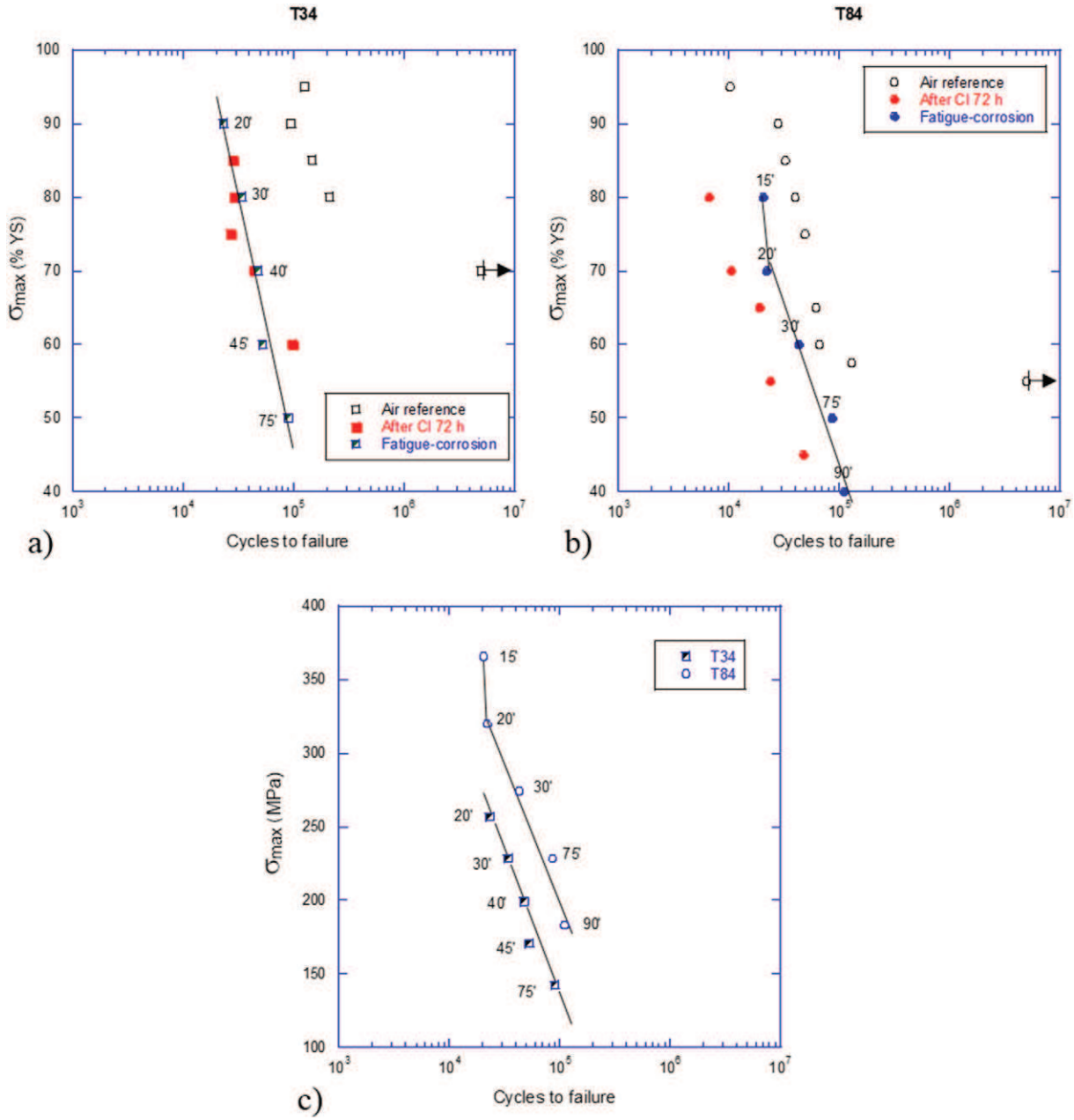

Fig. 10. Fatigue–corrosion life curves (σmax (% YS) vs. number of cycles to failure) of a) T34 and b) T84 metallurgical states at 20 Hz R = 0.1; and c) fatigue–corrosion life curves (σmax (MPa) vs. number of cycles to failure) of the T34 and T84 metallurgical states. For a) and b), results obtained for a 72 h pre-corroded sample are given for comparison.

Fig. 11. Observations by SEM of the fatigue–corrosion fracture surfaces of AA2050 tested at 20 Hz R = 0.1 for a stress level of 50% YS after a 72 h pre-corrosion treatment: a) T34 state; b) T84 state. White stars indicate the initiation zones.

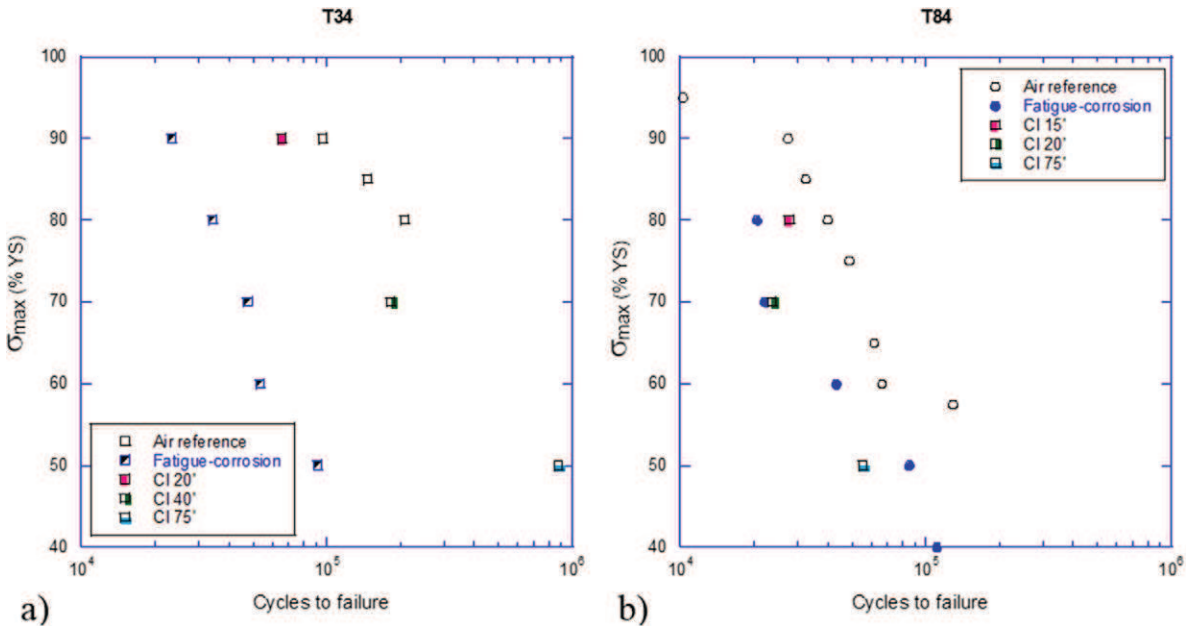

Fig. 12. Fatigue–corrosion life curves (σmax (% YS) vs. number of cycles to failure) of a) T34 and b) T84 metallurgical states at 20 Hz R = 0.1. On each graph, results obtained on pre-corroded samples (Cl) for short pre-immersion times are given for comparison.

intergranular corrosion, leading to a premature crack initiation and finally to the decrease in the fatigue life of the T34 metallurgical state.

4. Conclusion

The fatigue behaviour of AA2050 in two metallurgical states was studied in air for healthy and pre-corroded samples. The results were compared to those obtained during fatigue–corrosion tests in a 0.7 M NaCl solution.

Preliminary corrosion tests indicated that the T34 metallurgical state was susceptible to intergranular corrosion, while the T84 metallurgical state was susceptible to intragranular corrosion.

Fatigue life tests in air demonstrated that fatigue crack initiation was localised on coarse intermetallic particles for both microstructures. For both T34 and T84 metallurgical states, a crystallographic propagation was observed, characterised by flat-facets and step-like patterns related to an hydrogen effect in relation with microstructural characteristics of the material.

Fatigue life tests in air on pre-corroded samples revealed a decrease in the fatigue life related to the presence of corrosion defects before the cyclic solicitation. The effect of the first minutes of immersion in corrosive media on the fatigue life behaviour was clearly evidenced.

Concerning the fatigue–corrosion tests, the T34 metallurgical state was more affected by fatigue–corrosion in terms of fatigue life than the T84 metallurgical state. This observation should be explained, on the one hand, by the embrittlement of the passive oxide layer concerning both metallurgical states and, on the other hand, by the increased propagation of intergranular corrosion assisted by the cyclic solicitation. According to previous works on stress corrosion cracking, the mechanical solicitation appeared to favour the initiation and/or the propagation of a certain type of corrosion morphology by plasticity mechanisms at a very small scale.

Acknowledgements

The Région Midi-Pyrénées and PRES Université de Toulouse financially supported this work (MESR, 12051146). The authors thank Dr J. Delfosse (EADS IW, France) and Dr C. Henon (Constellium, France) for fruitful discussions.

References

[1] C. Meric, Physical and mechanical properties of cast under vacuum aluminum alloy 2024 containing lithium additions, Mater. Res. Bull. 35 (2000) 1479–1494.
[2] D. Tolga, S. Costas, Recent developments in advanced aircraft aluminium alloys, Mater. Des. 56 (2014) 862–871.
[3] J.E. Kertz, P.I. Gouma, R.G. Buchheit, Localized corrosion susceptibility of Al–Li–Cu–Mg–Zn alloy AF/C458 due to interrupted quenching from solutionizing temperatures, Metall. Mater. Trans. A 33 (2001) 2561–2573.
[4] N. Jiang, J.F. Li, Z.Q. Zheng, Effect of aging on mechanical properties and localized corrosion behaviors of Al–Cu–Li alloy, Trans. Nonferrous Met. Soc. China 15 (2005) 23–29.
[5] B. Decreus, A. Deschamps, F. De Geuser, P. Donnadieu, C. Sigli, M. Weyland, The influence of Cu/Li ratio on precipitation in Al–Cu–Li–x alloys, Acta Mater. 61 (2013) 2207–2218.
[6] J.F. Li, C.X. Li, Z.W. Peng, W.J. Chen, Z.Q. Zheng, Corrosion mechanism associated with T_1 and T_2 precipitates of Al–Cu–Li alloys in NaCl solution, J. Alloys Compd. 460 (2008) 688–693.
[7] J.F. Li, Z.Q. Zheng, W.D. Ren, W.J. Chen, X.S. Zhao, S.C. Li, Simulation on function mechanism of $T_1(Al_2CuLi)$ precipitate in localized corrosion of Al–Cu–Li alloys, Trans. Nonferrous Met. Soc. China 16 (2006) 1268–1273.
[8] R.G. Buchheit, J.P. Moran, G.E. Stoner, Electrochemical behavior of the $T_1(Al_2CuLi)$ intermetallic compound and its role in localized corrosion of Al-2% Li-3% Cu Alloys, Corrosion 50 (1994) 120–130.
[9] V. Proton, J. Alexis, A. Andrieu, J. Delfosse, M.-C. Laffont, C. Blanc, Characterization and understanding of the corrosion behaviour of the nugget in a 2050 aluminum alloy friction stir welding joint, Corros. Sci. 73 (2013) 130–142.
[10] R.G. Buchheit, J.P. Moran, G.E. Stoner, Localized corrosion behavior of alloy 2090—the role of microstructure heterogeneity, Corrosion 46 (1990) 610–617.
[11] F. Viejo, A.E. Coy, F.J. Garcia, Z. Liu, P. Skeldon, G.E. Thompson, Relationship between microstructure and corrosion performance of AA2050-T8 aluminum alloy after excimer laser surface melting, Corros. Sci. 52 (2010) 2179–2187.
[12] S. Richard, C. Gasqueres, C. Sarrazin-Baudoux, J. Petit, Coupled influence of microstructure and atmosphere environment on fatigue crack path in new generation Al alloys, Eng. Fract. Mech. 77 (2010) 1941–1952.
[13] G.S. Chen, K.C. Wan, M. Gao, R.P. Wei, T.H. Flournoy, Transition from pitting to fatigue crack growth-modeling of corrosion fatigue crack nucleation in a 2024-T3 aluminum alloy, Mater. Sci. Eng. A 219 (1996) 126–132.
[14] S.I. Roklin, J.Y. Kim, H. Nagy, B. Zoofan, Effect of pitting corrosion on fatigue crack initiation and fatigue life, Eng. Fract. Mech. 62 (1999) 425–444.
[15] K. Van der Walde, B.M. Hillberry, Initiation and shape development of corrosion-nucleated fatigue cracking, Int. J. Fatigue 29 (2007) 1269–1281.
[16] A.T. Kermanidis, P.V. Petroyiannis, Pantelakis SpG., Fatigue and damage tolerance behavior of corroded 2024 T351 aircraft aluminum alloy, Theor. Appl. Fract. Mech. 43 (2005) 121–132.
[17] K.M. Gruenberg, B.A. Craig, B.M. Hillberry, R.J. Bucci, A.J. Hinkle, Predicting fatigue life of pre-corroded 2024-T3 aluminum from breaking load tests, Int. J. Fatigue 26 (2004) 629–640.
[18] E.J. Dolley, B. Lee, R.P. Wei, The effect of pitting corrosion on fatigue life, *Fatigue Fract. Engng. Mater. Struct.* 23 (2000) 555–560.
[19] D.L. Du Quesnay, P.R. Underhill, H.J. Britt, Fatigue crack growth from corrosion damage in 7075-T6511 aluminum alloy under aircraft loading, Int. J. Fatigue 25 (2003) 371–377.

[20] N. Pauze, Fatigue corrosion dans le sens travers court de tôles d'aluminum 2024–T351 présentant des défauts de corrosion localisée, ENSM, Saint-Etienne: France, 2008 (Ph.D. thesis).
[21] A. Turnbull, Corrosion pitting and environmentally assisted small crack growth, Proc. R. Soc. Lond. A Math. Phys. Eng. Sci. 470 (2169) (2014).
[22] J.T. Burns, J.M. Larsen, R.P. Gangloff, Driving forces for localized corrosion to fatigue crack transition in Al–Zn–Mg–Cu, *Fatigue Fract. Engng. Mater. Struct.* 34 (2011) 745–773.
[23] J.T. Burns, S. Kim, R.P. Gangloff, Effect of corrosion severity on fatigue evolution in Al–Zn–Mg–Cu, Corros. Sci. 52 (2010) 498–508.
[24] V. Proton, J. Alexis, E. Andrieu, C. Blanc, J. Delfosse, L. Lacroix, G. Odemer, Influence of post-welding heat treatment on the corrosion behavior of a 2050 T3 aluminum–copper–lithium alloy friction stir welding joint, J. Electrochem. Soc. 158 (2011) C139–C147.
[25] M. Guérin, E. Andrieu, G. Odemer, J. Alexis, C. Blanc, Effect of varying conditions of exposure to an aggressive medium on the corrosion behavior of the 2050 Al–Cu–Li alloy, Corros. Sci. 85 (2014) 455–470.
[26] M. Guérin, Comportement en corrosion d'un alliage d'aluminum-cuivre-lithium AW2050: couplage environnement, microstructure et état de contrainte du matériau, INP, Toulouse: France, 2014 (Ph.D. thesis).
[27] M. Guérin, E. Andrieu, G. Odemer, J. Alexis, C. Blanc, The relationship between grain boundaries/grain properties and their corrosion susceptibility in a 2050 aluminium alloy, submitted to Corrosion Science (2015).
[28] J.G. Rinker, M. Marek, Microstructure, toughness and stress corrosion cracking behavior of aluminum alloy 2020, Mater. Sci. Eng. 64 (1984) 203–221.
[29] V. Proton, J. Alexis, E. Andrieu, J. Delfosse, A. Deschamps, F. De Geuser, M.-C. Lafont, C. Blanc, The influence of artificial ageing on the corrosion behaviour of a 2050 aluminium–copper–lithium alloy, Corros. Sci. 80 (2014) 494–502.
[30] Q. Contrepois, Texture et anisotropie du comportement mécanique après laminage à chaud d'un alliage léger d'aluminum cuivre lithium pour l'aéronautique, ENSM, Saint-Etienne: France, 2010 (Ph.D. thesis).
[31] V. Proton, J. Alexis, E. Andrieu, J. Delfosse, A. Deschamps, F. De Geuser, M.-C. Laffont, C. Blanc, The influence of artificial ageing on the corrosion behaviour of a 2050 aluminum–copper–lithium alloy, Corros. Sci. 80 (2014) 494–502.
[32] P. Lequeu, K.P. Smith, A. Danielou, Aluminum–copper–lithium alloy 2050 developed for medium to thick plate, J. Mater. Eng. Perform. 19 (2009) 841–847.
[33] Y. Ro, S.R. Agnew, G.H. Bray, R.P. Gangloff, Environment-exposure-dependent fatigue crack growth kinetics for Al–Cu–Mg/Li, Mater. Sci. Eng. A 468–470 (2007) 88–97.
[34] Y. Ro, S.R. Agnew, R.P. Gangloff, Unpublished Research, University of Virginia, Charlottesville, VA, 2006.
[35] D.C. Slavik, R.P. Gangloff, Environmental microstructure effects on fatigue crack facet orientation in an Al–Li–Cu–Zr alloy, Acta Metall. Mater. 44 (1996) 3515–3534.
[36] E.I. Meletis, W. Huang, The role of the T_1 phase in the pre-exposure and hydrogen embrittlement of Al–Li–Cu alloys, Mater. Sci. Eng. A 148 (1991) 197–209.
[37] N.J. Kim, E.U. Lee, Effect of T_1 precipitates on the anisotropy of Al–Li- alloy 2090, Acta Metall. Mater. 41 (1993) 941–948.
[38] K. Jones, D.W. Hoeppner, Prior corrosion and fatigue of 2024-T3 aluminum alloy, Corros. Sci. 48 (2006) 3109–3122.
[39] K. Vanderwalde, J. Brockenbrough, B. Craig, B. Hillberry, Multiple fatigue crack growth in pre-corroded 2024-T3 aluminum, Int. J. Fatigue 27 (2005) 1509–1518.
[40] S.I. Rokhlin, J. Kim, H. Nagy, B. Zoofan, Effect of pitting corrosion on fatigue crack initiation and fatigue life, Eng. Fract. Mech. 62 (1999) 425–444.
[41] X.D. Li, X.S. Wang, H.H. Ren, Y.L. Chen, Z.T. Mu, Effect of prior corrosion state on the fatigue small cracking behaviour of 6151-T6 aluminum alloy, Corros. Sci. 55 (2012) 26–33.
[42] S. Kim, J.T. Burns, R.P. Gangloff, Fatigue crack formation and growth from localized corrosion in Al–Zn–Mg–Cu, Eng. Fract. Mech. 76 (2009) 651–667.
[43] K.M. Gruenberg, B.A. Craig, B.M. Hillberry, Predicting fatigue life of pre-corroded 2024-T3 aluminum from breaking load tests, Int. J. Fatigue 26 (2004) 615–627.
[44] D. Delafosse, J.P. Chateau, A. Chambreuil, T. Magnin, Dislocation–hydrogen interactions during stress corrosion cracking in fcc metals: experiments on single crystals and numerical simulations, Mater. Sci. Eng. A 234 (1997) 889–892.